High-Order Residual-Distribution Schemes for Discontinuous Problems on Irregular Triangular Grids

Alireza Mazaheri*
NASA Langley Research Center, Hampton, VA 23681
Hiroaki Nishikawa†
National Institute of Aerospace, Hampton, VA 23666

In this paper, we develop second- and third-order non-oscillatory shock-capturing hyperbolic residual-distribution schemes for irregular triangular grids, extending our second- and third-order schemes [J. Comput. Phys., 300 (2015), 455–491] to discontinuous problems. We present extended first-order N- and Rusanov-scheme formulations for a hyperbolic advection-diffusion system, and demonstrate that the hyperbolic diffusion term does not affect the solution of inviscid problems for vanishingly small viscous coefficient. We then propose second- and third-order blended hyperbolic residual-distribution schemes with the extended first-order Rusanov-scheme. We show that these proposed schemes are extremely accurate in predicting non-oscillatory solutions for discontinuous problems. We also propose a characteristics-based nonlinear wave sensor for accurately detecting shocks, compression, and expansion regions. Using this proposed sensor, we demonstrate that the developed hyperbolic blended schemes do not produce entropy-violating solutions (unphysical shocks). We then verify the design order of accuracy of these blended schemes on irregular triangular grids.

I. Introduction

Accurate detection of discontinuities are of great interest to many practical applications. Equally, accurate prediction of solution and solution gradients in the smooth regions on irregular grids are also essential in estimating many important physical quantities such as viscous stress, vorticity, and heat flux. In Ref. 1, we presented new second- and third-order hyperbolic advection-diffusion schemes, and demonstrated that these schemes predict solution and solution gradients efficiently and accurately on anisotropic and irregular triangular grids. We then showed that these schemes do not require curved elements for geometries containing curved boundaries. We also showed that typically 10–15 residual evaluations are sufficient to obtain a converged solution with the proposed schemes. We developed these schemes by requiring the second- and the third-order schemes to preserve, respectively, quadratic and cubic exact solutions. These schemes are, however, not positive and may predict discontinuities, such as a shock, with over/undershoot values. Positivity requirement or some special treatment is needed to prevent an oscillatory solution around discontinuities.

Few approaches have been proposed that are widely used within the residual-distribution community to either construct a second-order positive scheme or combine a high-order non-positive scheme (typically second-order) with a first-order positive scheme. These are: (1) nonlinear advection schemes such as modified N-scheme or Positive-Streamwise-Invariant (PSI) scheme,[2] and limited schemes,[3] where a high-order smooth solution is recovered from a first-order positive scheme with a smoothness indicator, and (2) blended schemes,[4] in which a first-order and high-order schemes are blended through a nonlinear blending function. Although these approaches are different, one may recover an identical scheme from either of these approaches. These nonlinear schemes are first developed for the scalar advection equation and later extended for a system of equations. Despite their robustness, there are some drawbacks[5–8] in these schemes, such as poor and/or erratic iterative convergence, specially when they are applied to a system of equations. Thus, the formal

*Research Aerospace Engineer, Aerothermodynamics Branch, M/S 408A, Ali.R.Mazaheri@NASA.gov.
†Associate Research Fellow, 110 Exploration Way, Hampton, VA 23666.

high-order (typically second-order) accuracy of these schemes could not be guaranteed in smooth regions as obtaining a converged solution was a key ingredient in ensuring a high-order accurate solution in a smooth region. It was also reported in Ref. 8 that for implicit calculations, a first-order Jacobian must be used, otherwise CFL numbers in the order of unity need to be taken.

Here, we present alternative second- and third-order shock-capturing hyperbolic residual-distribution schemes for advection-diffusion problems on irregular grids that do not suffer from these shortfalls. This is done similar to the blending technique presented in Ref. 4 by combining our proposed non-positive second- and third-order hyperbolic advection-diffusion schemes (i.e., RD-CC2 and RD-CC3)[1] with a positive first-order hyperbolic advection-diffusion scheme, such as N or Rusanov, through a nonlinear blending function.

We also propose a technique, with which unphysical shocks or entropy-violating solutions are avoided with the help of the extended first-order Rusanov scheme. This approach requires accurate detection of sonic expansion. We perform this task by developing a new characteristics-based shock-sensor. The proposed characteristic-based shock sensor is an improvement to the technique reported in Refs. 9 and 10. The technique of Refs. 9 and 10, which uses divergence of characteristics as a mechanism to identify whether an element is in a shock, rarefaction, or away from such nonlinear waves, requires a threshold, and that is often very difficult to know a priori; a large threshold causes instability by high-order methods, while small thresholds lead compression waves to be treated as shocks, which in turn make the solution less accurate and undesirable. Here, we improve the previous technique with a more accurate characteristics-based shock-capturing operator that is less dependent on such thresholds. The proposed shock-capturing operator may also be used as a first step toward a development of a shock-fitting scheme.[11–13] In this present work, the characteristic-based shock-sensor is used as an alternative to a traditional entropy fix technique[14,15] to avoid unphysical shocks (entropy-violating solutions). Another alternative is to use a special quadrature formula,[10] but this technique requires development of completely new non-positive high-order schemes and therefore, was not pursued in this study.

In this paper, we focus on two-dimensional hyperbolic advection-diffusion systems and develop second- and third-order blended hyperbolic residual-distribution schemes for irregular triangular grids, extending the previous work[1] to discontinuous solutions. We first demonstrate that the hyperbolic diffusion terms do not negatively affect the solution of the advection equation as the diffusion coefficient approaches zero. We then demonstrate that these blended schemes can successfully detect physical discontinuities, and avoid unphysical shocks using the extended Rusanov scheme and a newly developed characteristics-based nonlinear wave sensor. Through numerical examples, we show that the proposed schemes not only provide an accurate solution but also give accurate and smooth solution gradients (away from discontinuities) on irregular grids that are otherwise not available with conventional schemes. This is extremely important because, as will be demonstrated, least squares reconstruction of gradients could be very inaccurate and oscillatory even if a high-order solution is used as a basis for the gradient reconstruction.

The paper is organized as follows. In Section II, we briefly describe the basics of a nonlinear hyperbolic advection-diffusion system. In Section III, we present extended first-order N and Rusanov schemes for a hyperbolic advection-diffusion system. In Section IV, we review the baseline RD, the RD-CC2 and RD-CC3 schemes that were proposed in Ref. 1; these schemes are used in construction of high-order blended schemes. Blended schemes are then presented in Section V. In Section VI, we discuss how entropy-violating solutions can be avoided. Boundary condition formulation is given in Section VII. We then present numerical examples in Section VIII, demonstrating the shock-capturing capability of the constructed second- and third-order blended hyperbolic advection-diffusion RD schemes on irregular triangular grids. Order of accuracy of these blended schemes are also verified in this section, followed by some concluding remarks in Section IX.

II. General nonlinear hyperbolic advection-diffusion system

Consider the following general two-dimensional nonlinear advection-diffusion equation:

$$\partial_t u + \partial_x f + \partial_y g = \partial_x(\nu \partial_x u) + \partial_y(\nu \partial_y u) + \tilde{s}(x, y, u), \tag{1}$$

where f and g are nonlinear functions of u, and $\nu = \nu(u)$. The advection speeds in x and y directions are therefore $a(u) = \partial f/\partial u$ and $b(u) = \partial g/\partial u$, respectively. We reformulate the advection-diffusion equation in the form of a nonlinear hyperbolic advection-diffusion system using a preconditioning matrix $\mathbf{P}$:

$$\mathbf{P}^{-1}\frac{\partial \mathbf{U}}{\partial \tau} + \frac{\partial \mathbf{F}}{\partial x} + \frac{\partial \mathbf{G}}{\partial y} = \mathbf{Q}, \tag{2}$$

where

$$\mathbf{P}^{-1} = \begin{bmatrix} 1 & 0 & 0 \\ 0 & T_r/\nu(u) & 0 \\ 0 & 0 & T_r/\nu(u) \end{bmatrix}, \quad \mathbf{Q} = \begin{bmatrix} s(x,y,u) \\ -p/\nu(u) \\ -q/\nu(u) \end{bmatrix}, \tag{3}$$

$$\mathbf{F} = \mathbf{F}^a + \mathbf{F}^d = \begin{bmatrix} f \\ 0 \\ 0 \end{bmatrix} + \begin{bmatrix} -p \\ -u \\ 0 \end{bmatrix}, \quad \mathbf{G} = \mathbf{G}^a + \mathbf{G}^d = \begin{bmatrix} g \\ 0 \\ 0 \end{bmatrix} + \begin{bmatrix} -q \\ 0 \\ -u \end{bmatrix}. \tag{4}$$

Note that the variables p and q are, in the pseudo steady state, equivalent to the diffusive fluxes in x and y directions, respectively. We also remark that, the physical time derivative can be incorporated into the source term s as shown in Ref. 16.

A computational domain is divided into a set $\{E\}$ of arbitrary triangular elements, E, and an associated set $\{J\}$ of nodes (or vertices). The total number of nodes in the computational domain is denoted as N, and the solutions (u_j, p_j, q_j) are stored at each node $j \in \{J\}$. We discretize the hyperbolic advection-diffusion system by the RD method, where the cell residual is computed over a triangular element as an integral approximation of the target equations, and then split and distributed to the three nodes. At the end of the process, we obtain the residual at a node as

$$\mathbf{Res}_j = \sum_{E \in \{E_j\}} \mathbf{\Phi}_j^E, \tag{5}$$

where $\{E_j\}$ denotes the set of triangles that share the node j, and $\mathbf{\Phi}_j^E$ is the split cell-residual contributing to the node j from the element E. The resulting global system of the nodal-residual equations is solved by the implicit solver with the residual Jacobian constructed based on a compact second-order scheme as described in Ref.[1] In general, the distributed cell-residual $\mathbf{\Phi}_j^E$ is defined such that

$$\sum_{j \in E} \mathbf{\Phi}_j^E = \mathbf{\Phi}^E, \tag{6}$$

where $\mathbf{\Phi}^E$ denotes the cell-residual over the element E. The RD scheme is characterized by the nodal contribution from each element, $\mathbf{\Phi}_i^E$. In the rest of the papers, therefore, we consider only $\mathbf{\Phi}_i^E$ and use the superscript to indicate the name of the scheme. The objective of the present work is to discretize the hyperbolic advection-diffusion system by combing a first-order scheme with high-order advection-diffusion schemes. In the next section, we discuss extended first-order advection-diffusion schemes, followed by a brief review of the second- and third-order schemes proposed in Ref. 1 in Sec. IV.

III. First-order advection-diffusion schemes

In this section, we present extensions of the first-order N and Rusanov scheme to advection-diffusion problems. We use these extended first-order schemes to construct second- and third-order blended hyperbolic advection-diffusion schemes in Sec. V. These first-order schemes are also used in Sec. VIII to study the effects of the hyperbolic diffusion term in the solution of discontinuous advection-diffusion problems as the diffusion coefficient approaches zero.

A. Advection-diffusion *N*-scheme

In this section, we directly extend the original first-order N scheme (aka Narrow) proposed in Refs. 17 and 18 for inhomogeneous advection equations to a general hyperbolic advection-diffusion system, by separating the advective and the diffusive terms of the cell residual using the non-unified technique we proposed in Ref. 1. We then combine the advective and the diffusive contributions to the nodal residual with a weighting function, and add them to the source term contribution of the cell residual to the node. The source term discretizations are performed in an analogous manner to the work of Ref. 6; i.e., utilize an alternative form of the N scheme as the second-order Low-Diffusion-A (LDA) scheme plus an anisotropic dissipation term. After some algebra, we arrive at

$$\mathbf{\Phi}_i^N = (1-\omega)\mathbf{\Phi}_i^a + \omega\mathbf{\Phi}_i^d + \mathbf{B}_i^{\text{LDA}}\mathbf{\Phi}_i^s, \tag{7}$$

where the advective, $\mathbf{\Phi}^a$, the diffusive, $\mathbf{\Phi}^d$, and the source term, $\mathbf{\Phi}^s$, contributions to the nodal residuals are:

$$\mathbf{\Phi}_i^a = -\mathbf{K}_i^{a+}(\mathbf{U}_i - \tilde{\mathbf{U}}^a), \tag{8}$$

$$\mathbf{\Phi}_i^d = -\mathbf{K}_i^{d+}(\mathbf{U}_i - \tilde{\mathbf{U}}^d) + \frac{1}{3}\mathbf{B}_i^{\mathrm{d}} \sum_{j\in E} \mathbf{Q}_j^d \, d\Omega^E, \tag{9}$$

$$\mathbf{\Phi}_i^s = \frac{1}{3}\sum_{j\in E} \mathbf{Q}_j^s \, d\Omega^E. \tag{10}$$

where the incoming field, $\tilde{\mathbf{U}}$, is defined also separately for the advection and the diffusion components as:

$$\tilde{\mathbf{U}}^a = \frac{\sum_{j\in E} \mathbf{K}_j^{a-}\mathbf{U}_j}{\sum_{j\in E} \mathbf{K}_j^{a-}} = -\frac{\sum_{j\in E} \mathbf{K}_j^{a-}\mathbf{U}_j}{\sum_{j\in E} \mathbf{K}_j^{a+}}, \quad \tilde{\mathbf{U}}^d = -\frac{\sum_{j\in E} \mathbf{K}_j^{d-}\mathbf{U}_j}{\sum_{j\in E} \mathbf{K}_j^{d+}}. \tag{11}$$

Following the work of Ref. 6, the LDA distribution matrices for the source terms become (see Ref.[19] for more details on the LDA distribution matrix for the hyperbolic advection-diffusion system):

$$\mathbf{B}_i^{\mathrm{LDA}} = \mathbf{K}_i^+ \left(\sum_{j=1}^{3} \mathbf{K}_j^+\right)^{-1}, \quad \mathbf{B}_i^d = \mathbf{K}_i^{+\,d} \left(\sum_{j=1}^{3} \mathbf{K}_j^{+\,d}\right)^{-1}. \tag{12}$$

We note that the hyperbolic diffusion source terms, $\mathbf{Q}^d$, are included as a part of the hyperbolic diffusion cell residual contribution to the node (i.e., $\mathbf{\Phi}_i^d$), while the contribution of the original advection-diffusion equation source term, $\mathbf{Q}^s$, to the node is defined as $\mathbf{\Phi}_i^s$. The matrix $\mathbf{K}_i$ corresponding to the preconditioned system is defined by

$$\begin{aligned}
\mathbf{K}_i &= \frac{1}{2}\overline{\mathbf{P}} \left(\overline{\frac{\partial \mathbf{F}}{\partial \mathbf{U}}}\hat{n}_{x_i} + \overline{\frac{\partial \mathbf{G}}{\partial \mathbf{U}}}\hat{n}_{y_i}\right)|\mathbf{n}_i|, \\
&= \frac{1}{2}\overline{\mathbf{P}} \left(\overline{\frac{\partial \mathbf{F}^a}{\partial \mathbf{U}}}\hat{n}_{x_i} + \overline{\frac{\partial \mathbf{G}^a}{\partial \mathbf{U}}}\hat{n}_{y_i}\right)|\mathbf{n}_i| + \frac{1}{2}\overline{\mathbf{P}} \left(\overline{\frac{\partial \mathbf{F}^d}{\partial \mathbf{U}}}\hat{n}_{x_i} + \overline{\frac{\partial \mathbf{G}^d}{\partial \mathbf{U}}}\hat{n}_{y_i}\right)|\mathbf{n}_i|, \\
&= \mathbf{K}_i^a + \mathbf{K}_i^d,
\end{aligned} \tag{13}$$

where the over-bar denotes a value evaluated by the arithmetic average of the solution $\mathbf{U}$ over the three nodes in the triangular element, and $\mathbf{n}_i = (n_{x_i}, n_{y_i})$ and $\hat{\mathbf{n}}_i = (\hat{n}_{x_i}, \hat{n}_{y_i})$ are, respectively, the scaled and unit inward normal vectors of the edge opposite to the node i in the triangular element. In Eqs. (8), (9), (11), we have decomposed the advective and the diffusive components of the $\mathbf{K}_i$ matrix according to the corresponding wave speeds (i.e., $\mathbf{K}_i = \mathbf{K}_i^+ + \mathbf{K}_i^-$), and used these equalities: $\sum_{j\in E} \mathbf{K}_j^a = \sum_{j\in E} \mathbf{K}_j^d = 0$.

Here, the weighting function ω is obtained based on a detailed analysis performed on a one-dimensional hyperbolic advection-diffusion system:[20]

$$\omega = \frac{2}{Re + 2}, \tag{14}$$

where we define the Re for the two-dimensional system as

$$Re = \sqrt{a^2 + b^2}/\nu. \tag{15}$$

Accordingly, $\omega \to 0$ as $Re \to \infty$, and $\omega \to 1$ as $Re \to 0$, and therefore, the extended N scheme proposed for the hyperbolic advection-diffusion system will properly reduce to pure advection and diffusion schemes as $Re \to \infty$ and $Re \to 0$, respectively.

B. Advection-diffusion *Rusanov* (Rv) scheme

The Rusanov scheme (aka Lax-Friedrichs)[21] is obtained from a centered scheme with an added isotropic dissipation term. In Ref. 6, it was shown that the Rusanov scheme is a positive and energy stable scheme, and thus, is suitable for construction of a blended scheme, which will be discussed in Sec. V. Here, we extend

the original advective Rusanov scheme to a general hyperbolic advection-diffusion system scheme with the same procedure we used for deriving the extended N scheme for hyperbolic advection-diffusion system; i.e., following the non-unified approach of Ref. 16, separating the advective and the diffusive parts of the cell residual, and then combining them with the weighting function ω, as defined in Eq. (14). The nodal residual can then be evaluated as

$$\mathbf{\Phi}_i^{\text{RV}} = (1-\omega)\mathbf{\Phi}_i^a + \omega\mathbf{\Phi}_i^d + \mathbf{\Phi}_i^s, \tag{16}$$

where the advective, $\mathbf{\Phi}^a$, the diffusive, $\mathbf{\Phi}^d$, and the source term, $\mathbf{\Phi}^s$, contributions to the nodal residuals are:

$$\mathbf{\Phi}_i^a = \frac{1}{3}\left(-\sum_{j\in E}\mathbf{K}_j^a\mathbf{U}_j\right) - \alpha^a(\mathbf{U}_i - \overline{\mathbf{U}}), \tag{17}$$

$$\mathbf{\Phi}_i^d = \frac{1}{3}\left(-\sum_{j\in E}\mathbf{K}_j^d\mathbf{U}_j + \mathbf{Q}_i^d d\Omega^E\right) - \alpha^d(\mathbf{U}_i - \overline{\mathbf{U}}), \tag{18}$$

$$\mathbf{\Phi}_i^s = \mathbf{Q}_i^s\frac{d\Omega^E}{3}, \tag{19}$$

where α^a and α^d are the spectral radii defined as

$$\alpha^a = max_{j\in E}(|\lambda_j^a|), \quad \alpha^d = max_{j\in E}(|\lambda_j^d|) = max_{j\in E}(\sqrt{\nu_j/T_r}), \tag{20}$$

with a note that the hyperbolic diffusion system is isotropic; i.e., $|\lambda_1^d| = |\lambda_2^d|$. It is clear that the scheme reduces to a scalar advection scheme in the advection-limit ($\omega \to 0$), and to a hyperbolic-diffusion system in the diffusion-limit ($\omega \to 1$).

IV. Second- and third-order hyperbolic RD schemes

In this section, we briefly review the second- and third-order schemes, namely the baseline, the RD-CC2, and the RD-CC3, presented in details in Ref. 1. These schemes are used here, in conjunction with the extended first-order schemes discussed earlier, to construct high-order blended schemes proposed in Sec. V. We first describe the cell-residuals for these schemes, and then present the SUPG distribution matrix that is used here to define the split cell-residual (or equivalently just to distribute the cell-residual) for all the schemes. Note that it is the cell-residual, not the distribution matrix, that characterizes the high-order schemes.

A. Second-order baseline RD scheme

The cell-residual for the preconditioned system, which is distributed to the element, is defined as

$$\mathbf{\Phi}^E = \begin{bmatrix} \Phi_u^E \\ \Phi_p^E \\ \Phi_q^E \end{bmatrix} = \overline{\mathbf{P}}\mathbf{\Psi}^E, \tag{21}$$

where the unpreconditioned cell–residuals $\mathbf{\Psi}^E$ is defined for Eq. (2) by

$$\begin{aligned} \mathbf{\Psi}^E = \begin{bmatrix} \Psi_u^E \\ \Psi_p^E \\ \Psi_q^E \end{bmatrix} &= \int_E (-\mathbf{F}_x - \mathbf{G}_y + \mathbf{Q})\, dx\, dy, \\ &= \sum_{j\in E}\left(-\frac{1}{2}\left(\mathbf{F}_j\hat{n}_{x_j} + \mathbf{G}_j\hat{n}_{y_j}\right)|\mathbf{n}_j| + \frac{1}{3}\mathbf{Q}_j d\Omega^E\right). \end{aligned} \tag{22}$$

B. Second-order RD-CC2 scheme

The solutions obtained with the baseline RD scheme[22] can be substantially improved by requiring the scheme to a preserve quadratic solution (and linear gradients). We called such a scheme RD-CC2 in Ref. 1. The second-order RD-CC2 scheme provides accurate and smooth solution gradients on arbitrary triangular grids that are otherwise less accurate and noisy with the baseline RD scheme. The cell residuals of the RD-CC2 can be expressed as the baseline RD scheme and added curvature correction terms, $\delta_i^{(\,)}$, as described in Ref. 1:

$$\tilde{\Phi}_u^E = \Phi_u^E - \frac{1}{2}\sum_{j\in E}\left(\delta_j^f n_{x_j} + \delta_j^g n_{y_j}\right), \tag{23}$$

$$\tilde{\Phi}_p^E = \Phi_p^E + \frac{\overline{\nu}}{2T_r}\sum_{j\in E}\delta_j^u n_{x_j}, \tag{24}$$

$$\tilde{\Phi}_q^E = \Phi_q^E + \frac{\overline{\nu}}{2T_r}\sum_{j\in E}\delta_j^u n_{y_j}, \tag{25}$$

Note that the curvature correction terms only depend on the solution gradients at the element vertices, which are available as part of the hyperbolic system formulation.

C. Third-order RD-CC3 scheme

The second-order RD-CC2 scheme was further extended by requiring the scheme to preserve a cubic solution (and quadratic gradients). The third-order scheme was designed as an add–on to the RD-CC2 scheme with additional curvature correction terms and high-order source discretization terms. We referred to this new third-order scheme as RD-CC3.[1] Briefly, the cell residual of the RD-CC3 scheme can be expressed as (see Ref. 1 for more details):

$$\tilde{\tilde{\Phi}}_u^E = \tilde{\Phi}_u^E + \frac{1}{2}\sum_{j\in E}\left(\delta_j^p n_{x_j} + \delta_j^q n_{y_j} - \frac{1}{2}\delta_j^s d\Omega^E\right), \tag{26}$$

$$\tilde{\tilde{\Phi}}_p^E = \tilde{\Phi}_p^E + \frac{\overline{\nu}}{4T_r}\sum_{j\in E}\delta_j^{p/\nu} d\Omega^E, \tag{27}$$

$$\tilde{\tilde{\Phi}}_q^E = \tilde{\Phi}_q^E + \frac{\overline{\nu}}{4T_r}\sum_{j\in E}\delta_j^{q/\nu} d\Omega^E. \tag{28}$$

We remark that the curvature correction terms in the RD-CC3 scheme are computed by the quadratic LSQ fit.

D. *SUPG* distribution scheme for advection-diffusion

In Ref. 1, we provided SUPG formulation for the hyperbolic advection-diffusion system using a non-unified approach, in which advective and diffusive terms are treated separately. Here, we briefly recall the formulation for completeness and provide some additional remarks.

Using the cell residuals evaluated from the baseline, the RD-CC2, or the RD-CC3 scheme, the nodal residual is obtained by distributing the cell residuals using a distribution matrix $\mathbf{B}$. Here, we use a SUPG scheme in the framework of RD for the construction of the distribution matrix:

$$\mathbf{\Phi}_i^{\text{SUPG}} = \mathbf{B}_i^{\text{SUPG}}\mathbf{\Phi}^E, \tag{29}$$

where the distribution matrix is computed by splitting the SUPG stabilization term in terms of advective and diffusive contributions as:

$$\mathbf{B}_i^{\text{SUPG}} = \frac{1}{3}\mathbf{I} + (1-\omega)\mathbf{D}_i^a + \omega\mathbf{D}_i^d, \tag{30}$$

where $\mathbf{I}$ is the identity matrix, and $\mathbf{D}_i^a$ and $\mathbf{D}_i^d$ are the stabilization terms defined independently for the advective and the diffusive terms,

$$\mathbf{D}_i^a = \begin{bmatrix} d_i^{\text{SUPG}} & 0 & 0 \\ 0 & 0 & 0 \\ 0 & 0 & 0 \end{bmatrix}, \quad d_i^{\text{SUPG}} = \frac{1}{2}\frac{a_{n_i}|n_i|}{\sum_{j\in E}\max(0,a_{n_j})|n_j|+\epsilon}, \tag{31}$$

$$\mathbf{D}_i^d = \frac{1}{2}\mathbf{K}_i^d\left(\sum_{j\in E}\mathbf{K}_j^{d+}\right)^{-1}, \tag{32}$$

and $a_n = \frac{\partial f}{\partial u}\hat{n}_x + \frac{\partial g}{\partial u}\hat{n}_y$. The $\epsilon \ll 1$ in the denominator of Eq. (31) is added to avoid division by zero when advection speed is identically zero.

The weighting function is defined in Eq. (14). We remark that although the effect of the weighting function was found to be insignificant for smooth solutions (see Ref. 1), we found it essential for cases with a discontinuous solution, such as the Burgers equation, to dampen solution gradients in the vicinity of discontinuities. The effect of the weighting function on the predicted solution is, however, insignificant.

V. Blended schemes

In this section, we combine a positive and monotone first-order hyperbolic RD scheme with our high-order hyperbolic advection-diffusion RD schemes using a blending parameter. Following the approach of Deconinck and van der Weide,[4] we propose the following blended scheme for general advection-diffusion problems:

$$\mathbf{\Phi}_i^{\text{B}} = \mathbf{\Theta}\mathbf{\Phi}_i^{\text{first-order}} + (\mathbf{I}-\mathbf{\Theta})\,\mathbf{\Phi}_i^{\text{high-order}}, \tag{33}$$

where $\mathbf{\Theta}$ is a blending matrix, $\mathbf{\Phi}_i^{\text{first-order}}$ is either the N or Rusanov scheme, and $\mathbf{\Phi}_i^{\text{high-order}}$ is either the RD baseline, the RD-CC2, or the RD-CC3 scheme; i.e., $\mathbf{\Phi}_i^{\text{SUPG}}$ with the corresponding cell-residual. The blending matrix $\mathbf{\Theta}$ is defined as

$$\mathbf{\Theta} = \begin{bmatrix} \theta_u & 0 & 0 \\ 0 & \theta_p & 0 \\ 0 & 0 & \theta_q \end{bmatrix}, \quad \theta_r = \frac{|\Phi_r^E|}{\sum_{j\in E}|\Phi_{r_j}^{\text{first-order}}|+\epsilon_\theta} \in [0,1], \tag{34}$$

where $r = u, p, q$ (corresponding to the advection and the hyperbolic diffusion equations), the cell residual Φ_r^E is evaluated with either the RD baseline, the RD-CC2, or the RD-CC3 scheme, and ϵ_θ is a constant introduced to avoid blending function to approach unity when both high-order and first-order cell residuals are vanishingly small. Here we have used $\epsilon_\theta = 10^{-4}$. Note that the hyperbolic diffusion contribution of the cell residual is included both in the high-order and the first-order residual evaluations used in Eq. (34). For better clarity, a letter "B" is appended to these schemes, and the corresponding resultant blending schemes are called RD-B, RD-CC2-B and RD-CC3-B, respectively.

We remark that the proposed blended schemes are for an advection-diffusion system, and that itself is significant, ensuring that formal order of accuracy of high-order schemes is recovered in the smooth region. Advection-only blended schemes are unlikely to recover the high-order solutions when it is applied to advection-diffusion systems, resulting in less accurate solutions in smooth regions.[23]

VI. Avoiding entropy-violating solutions (unphysical shocks)

It was shown in Ref. 15 that the RD method requires an entropy fix to ensure entropy satisfying expansion. There are few approaches in dealing with entropy-violating solutions. One approach is to modify the local wave speeds in the distribution matrix to break the symmetry that results in admitting unphysical shocks. This multi-dimensional entropy fix, proposed in Refs. 14 and 15, is identical, in one-dimensional cases, to a reformulation of the conventional entropy fix of Harten and Hyman.[24] Similar to the conventional entropy fix approach, the multi-dimensional entropy-fix technique is a global technique meaning that it is applied to the entire elements in the computational domain. Thus, detecting different regions of the flow field is not needed.

A different approach was proposed in Refs. 9 and 10 based on a special quadrature formula for the cell-residual that recognizes physically-correct changes in the entropy. This special quadrature formula can be used globally, but to capture physical shocks precisely (assuming one of the cell faces is aligned with the shock) a different quadrature formula must be used in the shock region. The use of different quadrature formulas in two adjacent elements will, then, require a fix over the common edge for conservation,[9,10] which is not very attractive as it makes the cell-residual evaluation non-local.

Here we propose an alternative approach in dealing with entropy-violating solutions. The proposed approach is based on activation of the first-order Rusanov scheme at the origin of the expansion shock. We will discuss this technique next, followed by a new characteristics–based nonlinear wave sensor to detect different regions of the flow field.

A. Avoiding unphysical shocks by the first-order Rusanov scheme

Many schemes are susceptible to unphysical shocks (entropy-violating solutions) and require an entropy fix technique to avoid them. In many cases, unphysical shocks are captured for the reason that the cell-residual vanishes or equivalently preserves such solutions, which often arises as a side effect of an accurate shock capturing capability. One way to avoid them is, therefore, to design the cell-residual such that it may vanish for shock waves, but does not vanish for unphysical shocks as in Refs. 9 and 10. In this work, however, we employ a much simpler strategy, noting that the first-order Rusanov scheme cannot preserve both physical and unphysical shocks. Namely, we design the proposed blended schemes such that they reduce to the first-order Rusanov scheme at the origin of the sonic expansion, and thereby avoid capturing unphysical shocks. We accomplish this by setting the blending parameter associated with the advection equation to one; i.e., $\theta_u = 1$. The proposed approach, therefore, requires accurate detection of the unphysical shocks. In the next section, we propose and explain in details a characteristics-based approach to accurately detect different regions of the flow field, including the sonic expansion regions.

B. Characteristics-based nonlinear wave sensor

We propose a technique based on the characteristic waves to identify nonlinear waves: shocks, compression, and expansion regions within a domain. The proposed method is a great improvement over the technique reported in Refs. 9 and 10 with minimal dependency on thresholding parameters and superiority in predicting various regions. The proposed approach may be used to mark the elements containing shock lines (or surfaces in 3D) and/or are within the compression or expansion regions. Initially, we used this information to construct a characteristics-based blending function, but observed that some thresholding parameter should be introduced to reduce the predicted overshoot and/or undershoot values around discontinuities. Note that the proposed sensor is not just a shock sensor; it is a more general sensor that detects various nonlinear waves such as compression and expansion waves as well. We also remark that the proposed technique is also applicable in constructing a shock fitting technique,[12,13] which will be discussed in future reports.

Consider an element E with an area of S^E, located either in the compression, expansion, or shock region (see Fig. 1). If we allow the vertices of the element to travel along the characteristic lines with the wave

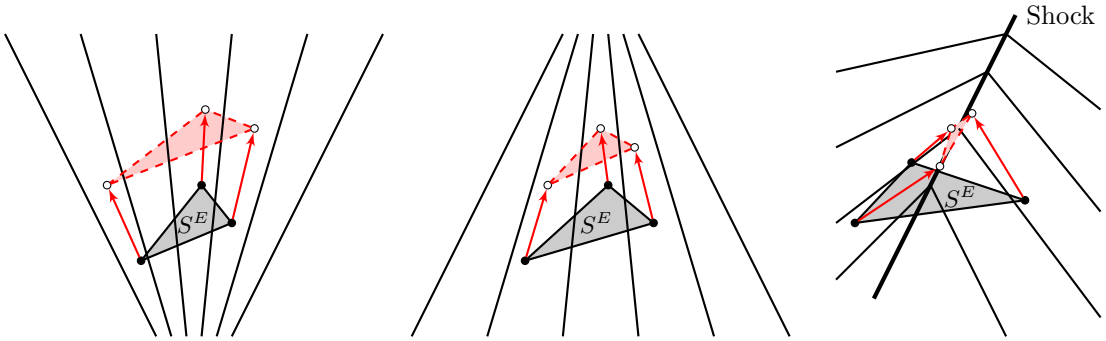

(a) Expansion; $dS^E/d\tau > 0$ (b) Compression; $dS^E/d\tau < 0$ (c) Shock; $dS^E/d\tau < 0$

Figure 1. Schematics of movements of an element E along the characteristics lines in the expansion, compression, and shock regions.

speed λ, we can obtain the rate of change of the element area as:

$$\frac{dS^E}{d\tau} = \text{ div } \vec{\lambda}\, S^E = \frac{1}{2}\sum_{j\in E} \vec{\lambda_j} \cdot \mathbf{n}_j, \tag{35}$$

As discussed in Refs. 9 and 10, this quantity is negative if the element is inside a shock wave with converging characteristics, and therefore the area will vanish (and then go negative) for shocks. In Refs. 9 and 10, the above quantity is directly employed with a simple normalization as a sensor for detecting shocks and sonic expansions. Here, we consider an alternative normalization based on the distance D_0 at which the element travels with the characteristic speed, λ, until element area becomes zero. Suppose the time it takes to reach an element with a zero area (or volume in 3D) is τ. Then, we can integrate Eq. (35) to get

$$0 - S^E = \tau \frac{1}{2}\sum_{j\in E} \vec{\lambda_j} \cdot \mathbf{n}_j. \tag{36}$$

Solving for τ, we obtain

$$\tau = \frac{-2\, S^E}{\sum_{j\in E} \vec{\lambda_j} \cdot \mathbf{n}_j}, \tag{37}$$

which corresponds to the following distance at which the element area vanishes:

$$D_0 = |\tau \vec{v}| = \tau |\vec{v}|, \tag{38}$$

where $\vec{v}$ is the average speed of the element; i.e., $\vec{v} = 1/3 \sum_{j\in E} \vec{\lambda}_j$.

Consider now $\overline{h}$ as a distance across the element E taken by the averaged characteristic speed $\vec{v}$. That is:

$$\overline{h} = |p_{out} - p_{in}|, \tag{39}$$

where p_{in} and p_{out} are the coordinates of the inflow and outflow as depicted in Fig. 2, which can be evaluated

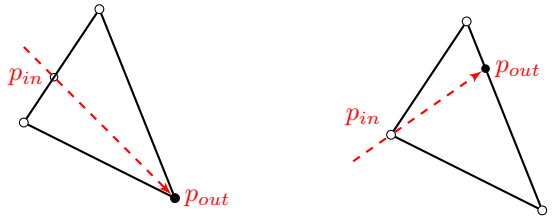

(a) one-target case (b) two–target case

Figure 2. Schematic of one- and two-target cases, corresponding to one and two upwind nodes, in defining $\overline{h}$.

(similar to the LDA technique) as

$$p_{in} = \frac{\sum_{j\in E} k_j^- p_j}{\sum_{j\in E} k_j^-}, \quad p_{out} = \frac{\sum_{j\in E} k_j^+ p_j}{\sum_{j\in E} k_j^+}, \tag{40}$$

where

$$k_i = \frac{1}{2}\vec{v} \cdot \mathbf{n}_i, \quad k_i^+ = max(0, k_i), \quad k_i^- = min(0, k_i). \tag{41}$$

Substituting Eq. (40) into Eq. (39), we arrive, after some algebra, at the following formulation:

$$\overline{h} = \frac{S^E}{\sum_{j\in E} k_j^+} |\vec{v}|, \tag{42}$$

where we have noted that $k_j = k_j^- + k_j^+$ and $\sum_{j\in E} n_{x_j} x_j = \sum_{j\in E} n_{y_j} y_j = 2S^E$.

Comparing the distance D_0 with the distance $\overline{h}$, which is the distance across the element taken by the averaged characteristic speed, we propose the following criteria for various regions of the flow field according to the value of $\alpha = \overline{h}/D_0$ ratio:

$$\alpha = \frac{-\sum_{j\in E} \vec{\lambda_j} \cdot \mathbf{n}_j}{2\sum_{j\in E} k_j^+} = \begin{cases} \geq 1 & \text{shock} \\ 0 < \ldots < 1 & \text{compression} \\ -1 < \ldots \leq 0 & \text{expansion} \\ \leq -1 & \text{sonic expansion} \end{cases} \tag{43}$$

Figure 3 shows computed α sensor within the entire domain from a sample solution of a nonlinear viscous Burgers equation on a 64×64 irregular grid $\in (0, 1.5)\times(0, 1)$ with $u(x, 0) = 1.5-2x$ as a boundary condition.

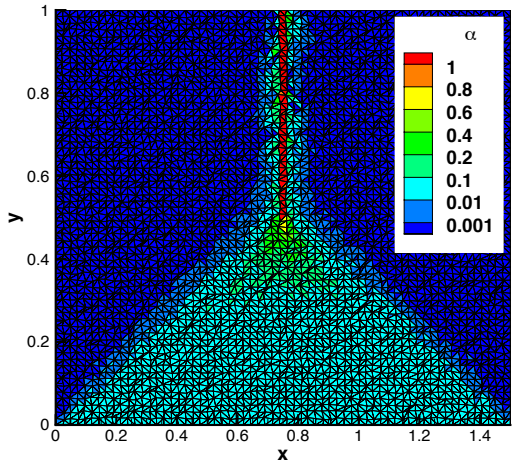

Figure 3. Elemental value of α sensor computed for a sample nonlinear viscous Burgers equation with 64×64 irregular grids.

We now summarize the discussion with a step-by-step procedure for a general advection equation (i.e., $u_t + f_x + g_y = 0$) as following:

- loop over elements
- evaluate $\vec{\lambda} = (f_u, g_u)$ for every vertex. For example, for Burgers equation, we have $\vec{\lambda} = (u, 1)$
- evaluate average speed of the element $\vec{v} = 1/3\left(\sum_j (f_u)_j, \sum_j (g_u)_j\right)$. For Burgers equation, we get $\vec{v} = \left(1/3\sum_j u_j, 1\right)$
- evaluate $k_j^+ = 1/2 \max\left(0, \vec{v}\cdot(n_{x_j}, n_{y_j})\right)$
- evaluate $\sum_j \vec{\lambda_j} \cdot (n_{x_j}, n_{y_j})$
- evaluate α as given in Eq. (43)
- set $\theta_u = 1.0$ for $\alpha \leq -0.9$ to avoid unphysical shocks; note that in Eq. (43) $\alpha \leq -1.0$ corresponds to the sonic expansion region but the actual computed α value, due to some numerical errors, may not be precisely ≤ -1.0. Therefore, we propose $\alpha \leq -0.9$. We also note that the entropy-violating phenomena is an advection problem and therefore, we do not modify the blending parameters associated with the hyperbolic diffusion terms (i.e., θ_p and θ_q); modification to the blending parameters θ_p and θ_q will destroy the accuracy of the predicted solution gradients.

The above procedure is used as a part of the shock-capturing hyperbolic blended schemes discussed in Sec. V. We remark that the proposed shock-capturing technique can also be directly used for development of a shock-fitting scheme, which is beyond the scope of the present study, and therefore, will be investigated in the future.

VII. Boundary condition

The details of formulating strong boundary condition for a hyperbolic residual-distribution scheme are reported in Ref. 1. Imposing a strong BC is not possible for some boundaries and, instead, a weak formulation needs to be constructed. For the cases we studied here, the outflow boundary is implemented with the weak formulation using ghost cells with vanishing volume. The weak outflow BC formulation is explained in details in the following subsection.

A. *Weak* outflow boundary condition

We start the process by creating as many virtual ghost elements as boundary nodes. This is done by adding a node in an opposite direction of the boundary face normals, such that the ghost element is an element with a 90-degree angle as shown in Fig. 4a. Depending on the boundary type, we can use different values in the

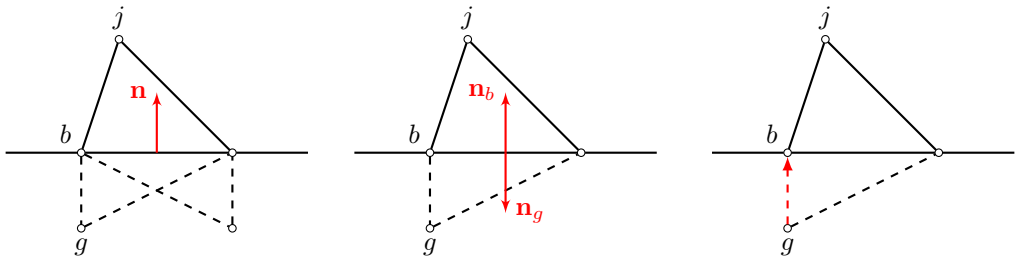

(a) Step 1: ghost element (b) Step 2: residual evaluation (c) Step 3: approaching g to b

Figure 4. Schematic of the weak boundary condition process using ghost elements. Steps 2 and 3 are illustrated for the left node. The same is repeated for the right node as illustrated in Step 1.

ghost nodes. For the outflow boundary condition, which is the only weak BC we studied here, we simply use the same information that is available from the vertex of the boundary element that is not on the boundary. This step is schematically shown in Fig. 4b:

$$\mathbf{U}_g = \mathbf{U}_j, \tag{44}$$

where subscript g denotes the ghost vertex. We then formulate the extended N scheme described in Sec. A while simultaneously allowing vertex g to approach vertex b, which is the boundary node, to form a zero-volume ghost cell (see Fig. 4c). The ghost cell contribution to the boundary node residual, after some algebra, becomes

$$\mathbf{\Phi}_b = -(1-\omega)\,\mathbf{K}_b^{a+}(\mathbf{U}_b - \mathbf{U}_g) - \omega\,\mathbf{K}_b^{d+}(\mathbf{U}_b - \mathbf{U}_g). \tag{45}$$

where we have used the geometrical relation $\mathbf{n}_g = -\mathbf{n}_b$, and adapted the same non-unified approach and the weighting function given in Eq. (14) for the boundary nodes. We remark that, because of the presence of $\mathbf{K}^+$, the above formulation allows only the incoming information to the domain to be included on the boundary. The presented formulation is different than other weak boundary condition formulations[15,25] because both the advective and the diffusive components are accounted for in this proposed formulation.

Note that the ghost cell residual contribution to the boundary nodes, $\mathbf{\Phi}_b$, is added to the boundary nodal residuals computed from the interior schemes. The corresponding Jacobian contribution, obtained with the use of *Automatic Differentiation* through an operator overloading technique using chain rules, is also added to the Jacobian computed for the interior nodes.

VIII. Results

All examples presented in this section are solved on a series of irregular and perturbed grids, unless otherwise stated. A representative of an irregular mesh is shown in Fig. 5. The implicit solver as described

in Ref.[1] is used to solve the nodal-residual equations. The linear relaxation is performed with a Gauss-Seidel algorithm to reduce the linear residuals by two orders of magnitude with a maximum of 1000 relaxation steps. The implicit solver is considered to be converged when ten orders of magnitude residual reduction is obtained for all the equations. To avoid instability with the implicit solver, full Newton update is not allowed at the beginning of the simulations (typically 20–30 Newton iterations). After the initial steps, a full Newton update is performed, which results in a converged solution typically in 5–15 additional Newton iterations.

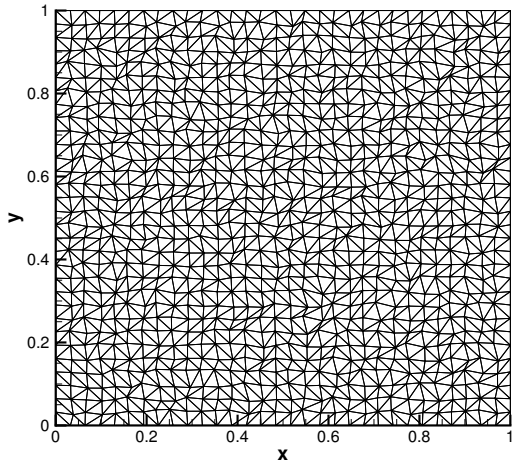

Figure 5. A representative of a perturbed and irregular grid used in all the presented examples (unless otherwise stated).

In this section, we seek the following objectives, which are addressed in the next subsections:

- the hyperbolic formulation of viscous terms does not negatively affect the solution of the inviscid equation as the viscosity coefficient approaches zero,
- a weak outflow boundary condition is implemented correctly,
- the proposed blended hyperbolic RD schemes can accurately capture discontinuity,
- non-physical shocks (e.g., sonic expansion) can be avoided by the proposed technique,
- the formal order of accuracy of the proposed blended schemes are preserved in smooth regions.

A. Hyperbolic advection-diffusion system vs. scalar advection

Consider the following nonlinear viscous Burgers equation

$$\partial_t u + \partial_x \left(\frac{u^2}{2}\right) + \partial_y u = \nu(\partial_{xx} u + \partial_{yy} u) \tag{46}$$

$$u(x,y) = 1.5 - 2x, \quad \text{on } y = 0. \tag{47}$$

The problem has the following exact solution in $(x,y) \in [0,1]\times[0,1]$ as $\nu \to 0$:

$$u(x,y) = \begin{cases} \text{for } y \geq 0.5, & \begin{cases} -0.5, & \text{if } -2\,(x-0.75) + (y-0.5) \leq 0, \\ 1.5, & \text{else,} \end{cases} \\ \text{otherwise,} & \max\left(-0.5, \min\left(1.5, \frac{x-0.75}{y-0.5}\right)\right). \end{cases} \tag{48}$$

We solve the above equation using scalar advection schemes (N, Rusanov, and the baseline RD with SUPG distribution) and compare them with the solutions of the hyperbolic advection-diffusion system formulation for vanishingly small diffusion coefficient ($\nu = 10^{-6}$). To remove the effects of weak outflow boundary

condition formulation (if any) and better characterize the hyperbolic system formulation against the scalar advection schemes, we employed a strong boundary condition that was described in Ref. 1. The results of this exercise are presented in Fig. 6, which shows that the hyperbolic advection-diffusion system formulation with vanishingly small diffusion coefficient (shown as Hyp-ADE) produces almost identical results as the scalar advection schemes. These results verify that the hyperbolic advection-diffusion formulation does not

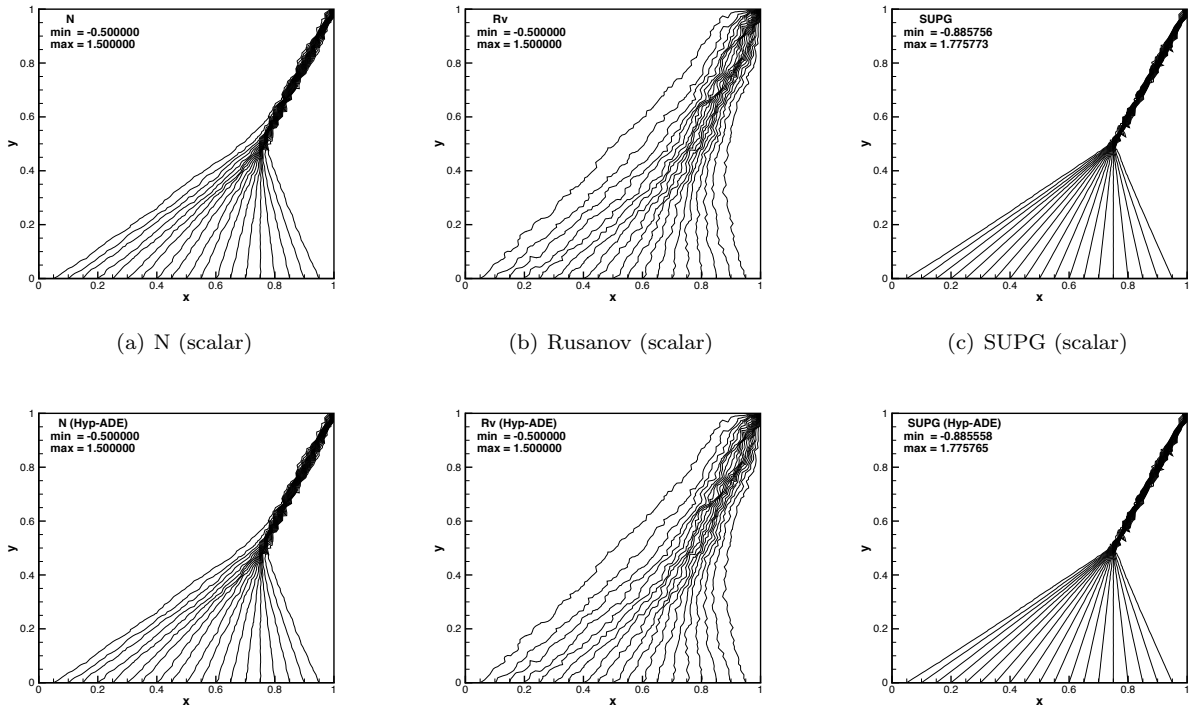

(a) N (scalar) (b) Rusanov (scalar) (c) SUPG (scalar)

(d) N (hyperbolic system) (e) Rusanov (hyperbolic system) (f) SUPG (hyperbolic system)

Figure 6. Comparison between the scalar advection schemes (first row), and the non-blended hyperbolic advection-diffusion (Hyp–ADE) schemes with $\nu = 1 \times 10^{-6}$ (second row) for the Burgers problem in $(x, y) \in$ [0,1]×[0,1] with a 64×64 irregular and perturbed grid.

affect the solution of the inviscid solution as viscosity coefficient approches zero. In the following examples, therefore, only the hyperbolic advection-diffusion system formulation is used. Note that in this example, the blending formulation is not used and therefore, it is expected that the second-order baseline RD scheme to predict some under/overshoots around the discontinuity, which are present in both scalar advection and hyperbolic system results.

B. Verification of weak outflow BC

Consider the nonlinear viscous Burgers equation, Eq. (46), along with the boundary condition given in Eq. (47) in $(x, y) \in [0,1.5]\times[0,y_{max}]$ domain, which results in a formation of a normal shock along the $x = 0.75$ plane. Here, three y_{max} values of 0.4, 0.6, and 1.0 are considered. A 64×64 irregular and perturbed triangular grid was generated for the largest domain (i.e., $y_{max} = 1.0$) as the basis mesh. Then, smaller grid sizes for the other two domains are generated such that the number of grid points in the y-direction becomes approximately proportional to the y_{max} value. For example, a 64×25 grid is generated for the domain with $y_{max} = 0.4$ ($64 \times 0.4 \sim 25$). Similarly, a grid size of 64×38 is generated for the domain with $y_{max} = 0.6$ ($64 \times 0.6 \sim 38$). This is to ensure that the truncated solution can be produced with the corresponding truncated grid system, verifying the accuracy of the weak outflow boundary condition. We use the hyperbolic advection-diffusion system and solve the above problem using the baseline RD scheme with the proposed weak outflow boundary condition applied at $y = y_{max}$ as shown in Fig. 7.

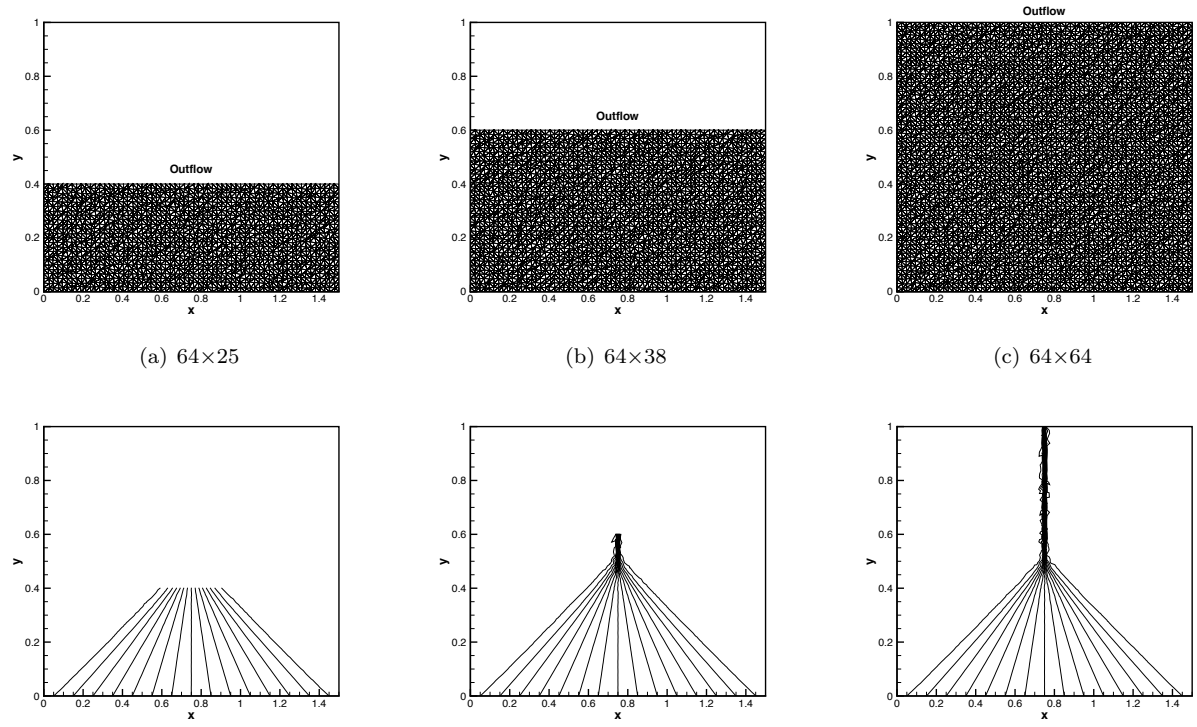

(a) 64×25 (b) 64×38 (c) 64×64

(d) $(x, y) \in (0,1.5)\times(0,0.4)$ (e) $(x, y) \in (0,1.5)\times(0,0.6)$ (f) $(x, y) \in (0,1.5)\times(0,1.0)$

Figure 7. Verification of the weak outflow BC formulation for the hyperbolic RD scheme. Solutions are for the viscous Burgers problem with irregular and perturbed grids.

C. Blended hyperbolic advection-diffusion schemes

In this example, we compare solutions of the viscous Burgers equation, Eq. (46), along with the boundary condition given in Eq. (47) predicted with the proposed blended hyperbolic advection-diffusion schemes constructed based on the presented first-order N and Rusanov (Rv) schemes (see Sec. III). Figure 8 shows solutions obtained with the blended baseline RD, RD-CC2 and RD-CC3 schemes, called, respectively, RD-B, RD-CC2-B, and RD-CC3-B. The converged solutions are obtained by freezing the blending parameter, $\mathbf{\Theta}$, after a certain number of Newton iterations, typically 30–35, otherwise we experienced that the residuals may plateau, typically around 10^{-7} value. The results show that the proposed blended hyperbolic schemes accurately predict both the compression waves and the discontinuity.

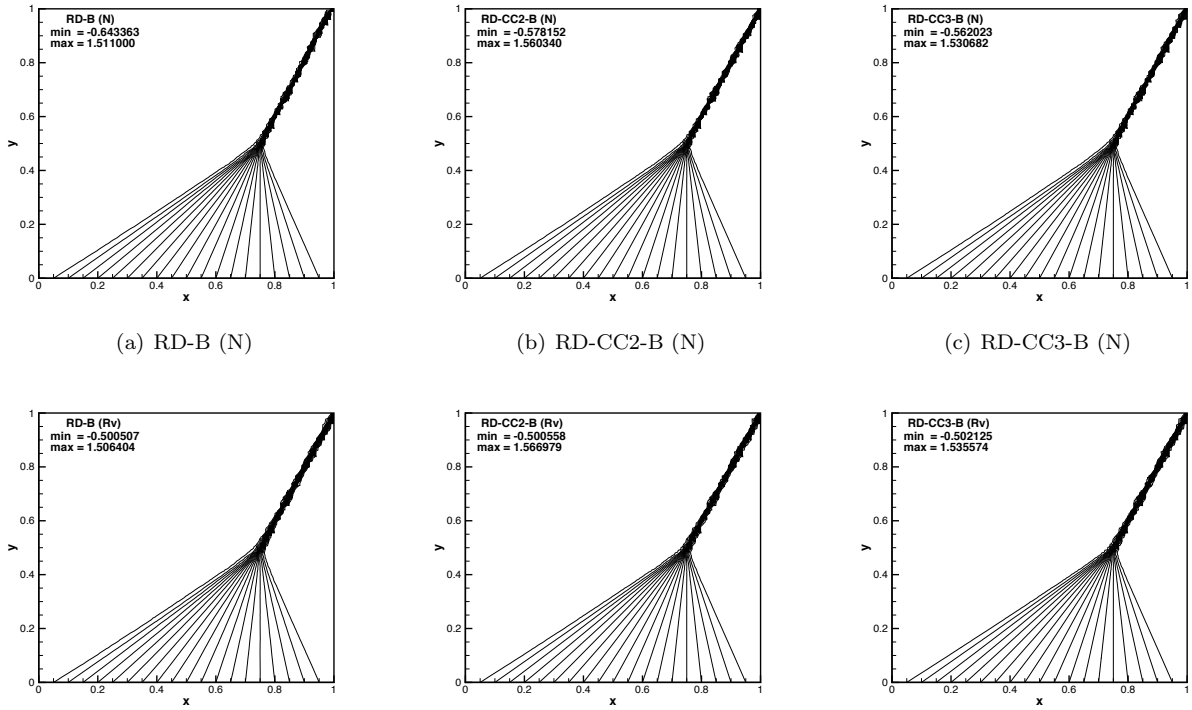

(a) RD-B (N) (b) RD-CC2-B (N) (c) RD-CC3-B (N)

(d) RD-B (Rv) (e) RD-CC2-B (Rv) (f) RD-CC3-B (Rv)

Figure 8. Comparison between the proposed N–based (first-row) and Rusanov–based (second-row) blended hyperbolic RD schemes applied to the Burgers problem in $(x, y) \in$ [0,1]×[0,1] on 100×100 irregular and perturbed grid.

The predicted solution with the proposed Rusanov-based blended schemes across the shock at $y = 0.6$ as well as the solution and the solution gradients across the compression region at $y = 0.3$ are compared with the corresponding exact values in Fig. 9. The solution across the shock is accurately detected with no oscillation. The accuracy of the RD-CC2-B and the RD-CC3-B schemes are more evident in the compression region. The proposed blended RD-CC2-B scheme predicts a solution and solution gradients that are significantly more accurate than the baseline RD-B scheme. Even though the second-order RD-CC2 scheme approaches the third-order accurate RD-CC3 solution for small viscosity coefficient as shown in Ref. 1, the improved solution gradients predicted by the blended RD-CC3-B scheme is remarkably noticeable. The proposed blended hyperbolic schemes, therefore, enable accurate prediction of solution gradients across the expansion fan that are otherwise not available with conventional schemes. For comparison, we have also computed solution gradients reconstructed using quadratic least-squares and compared them with the predicted values. As shown, the reconstructed solution gradients are oscillatory and inaccurate even if a high-order (in this case, third-order) solution is used.

The results of the proposed N-based blended schemes are comparable with the Rusanov-based blended schemes. A more detailed comparison between the proposed N-based and the Rusanov-based blended schemes is shown in Fig. 10 for the third-order RD-CC3-B schemes. Similar comparisons are obtained with the RD-B

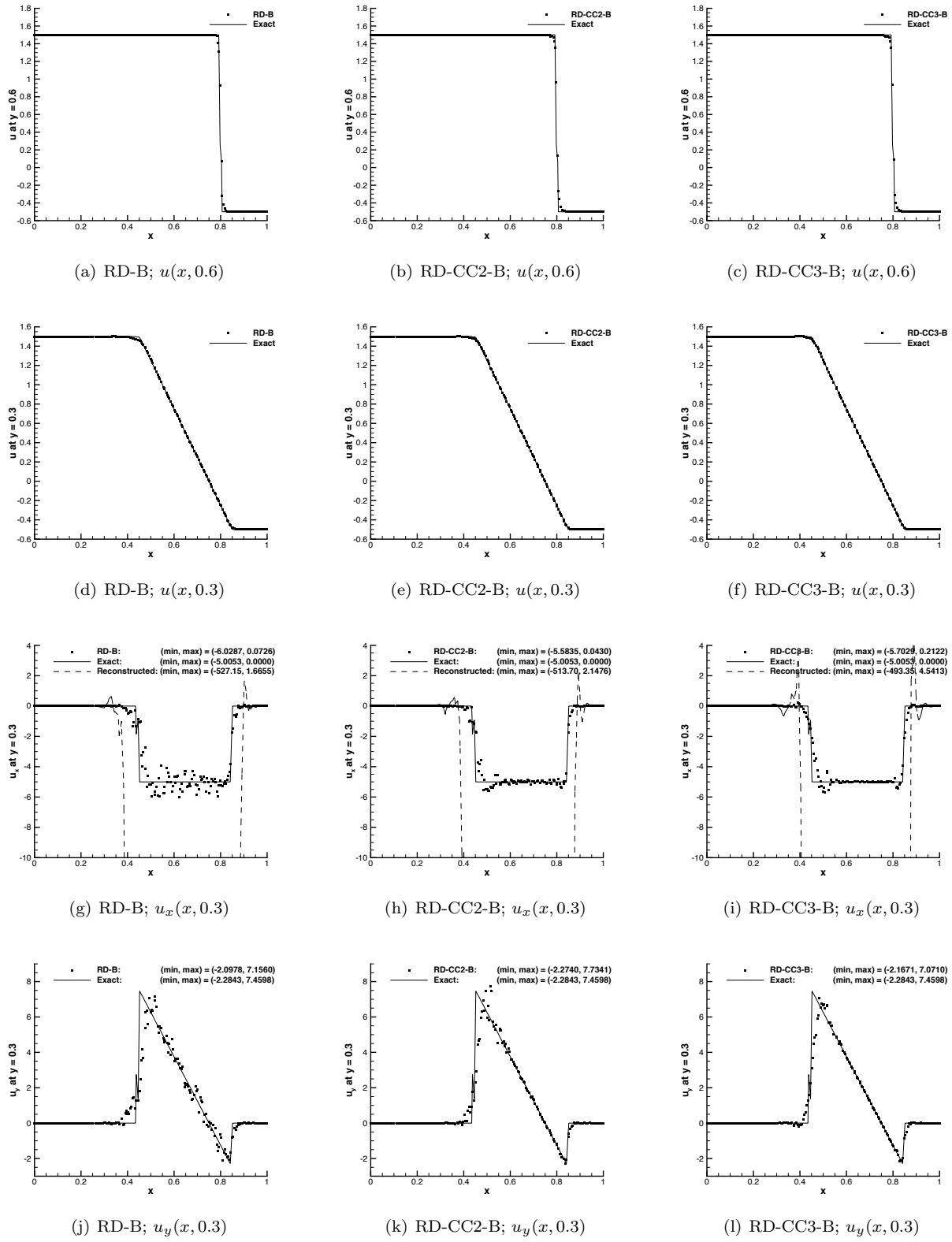

(a) RD-B; $u(x, 0.6)$ (b) RD-CC2-B; $u(x, 0.6)$ (c) RD-CC3-B; $u(x, 0.6)$

(d) RD-B; $u(x, 0.3)$ (e) RD-CC2-B; $u(x, 0.3)$ (f) RD-CC3-B; $u(x, 0.3)$

(g) RD-B; $u_x(x, 0.3)$ (h) RD-CC2-B; $u_x(x, 0.3)$ (i) RD-CC3-B; $u_x(x, 0.3)$

(j) RD-B; $u_y(x, 0.3)$ (k) RD-CC2-B; $u_y(x, 0.3)$ (l) RD-CC3-B; $u_y(x, 0.3)$

Figure 9. Comparison between the proposed Rusanov–based blended hyperbolic RD schemes for the Burgers problem in $(x, y) \in$ [0,1]×[0,1] on 100×100 irregular and perturbed grids. First-row: $u(x, 0.6)$, second-row: $u(x, 0.3)$, third-row: $u_x(x, 0.3)$, forth-row: $u_y(x, 0.3)$.

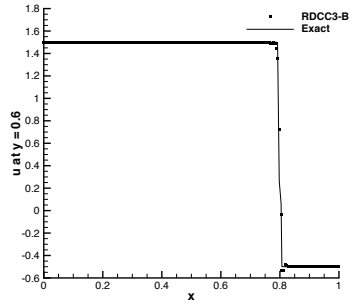

(a) N-based; $u(x, 0.6)$

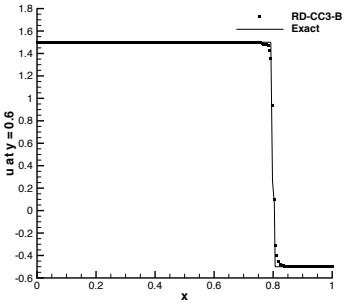

(b) Rusanov-based; $u(x, 0.6)$

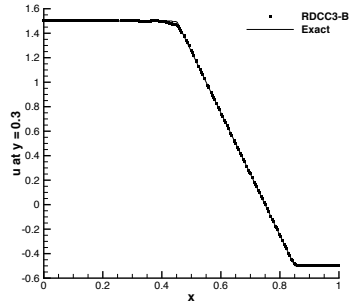

(c) N-based; $u(x, 0.3)$

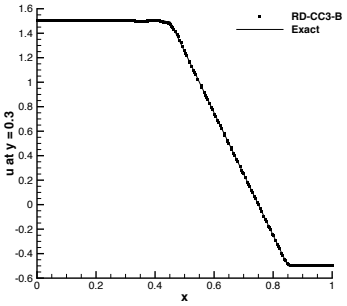

(d) Rusanov-based; $u(x, 0.3)$

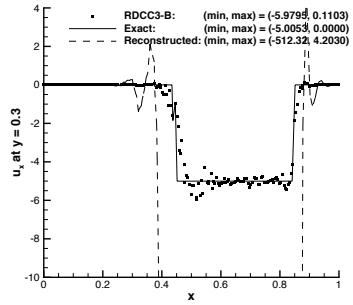

(e) N-based; $u_x(x, 0.3)$

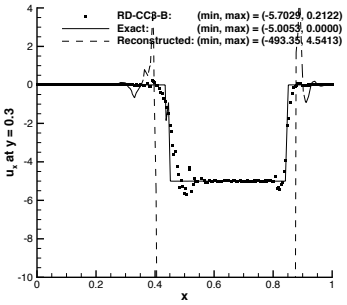

(f) Rusanov-based; $u_x(x, 0.3)$

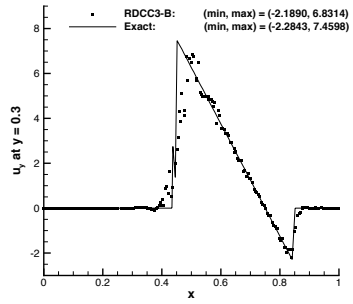

(g) N-based; $u_y(x, 0.3)$

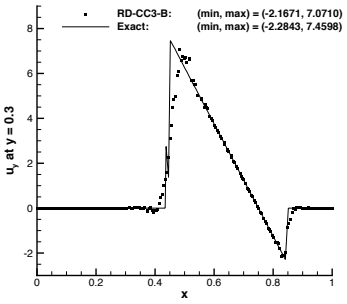

(h) Rusanov-based; $u_y(x, 0.3)$

Figure 10. Comparison between the proposed N-based and Rusanov–based blended hyperbolic RD-CC3 scheme for the Burgers problem in $(x, y) \in$ [0,1]×[0,1] on 100×100 irregular and perturbed grids. First-row: $u(x, 0.6)$, second-row: $u(x, 0.3)$, third-row: $u_x(x, 0.3)$, forth-row: $u_y(x, 0.3)$.

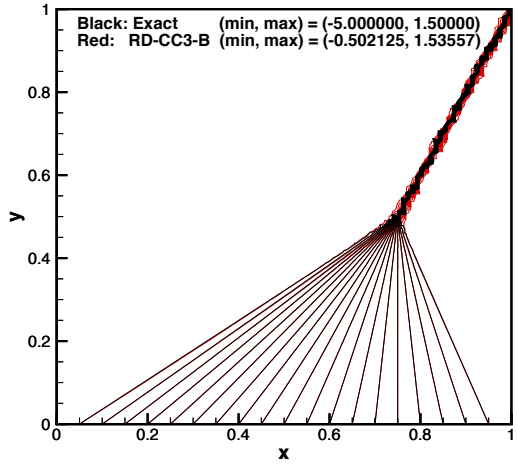

(a) Solution u

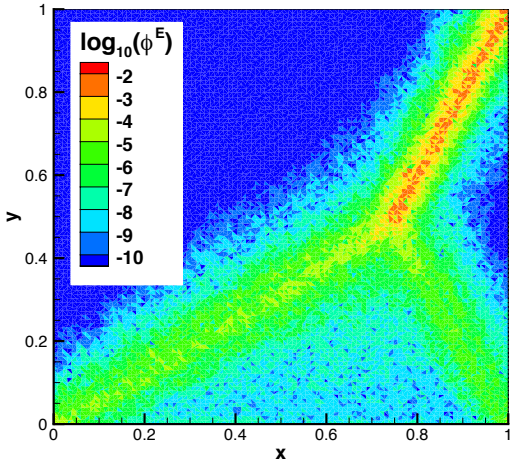

(b) Elemental residual

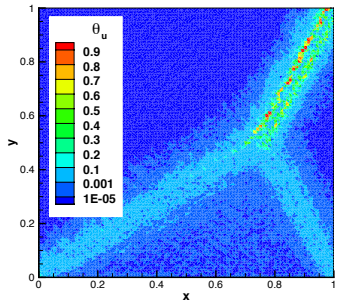

(c) Blending indicator θ_u

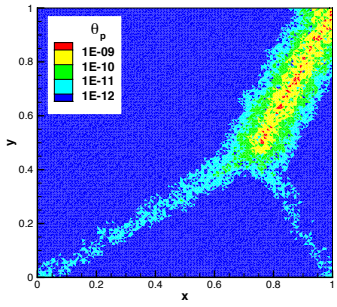

(d) Blending indicator θ_p

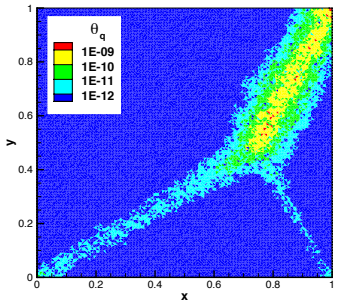

(e) Blending indicator θ_q

Figure 11. Elemental residual and blending indicators based on the proposed blended hyperbolic RD schemes for the Burgers problem in $(x, y) \in$ [0,1]×[0,1] on 100×100 irregular and perturbed grids (Note: Nodal residuals are converged to less than 10^{-10}).

and the RD-CC2-B schemes, and therefore, not shown. The predicted solution by the N-based scheme across the shock at $y = 0.6$ is slightly more accurate (sharper) than the Rusanov-based solution, but the N-based blended scheme predicts a slight undershoot on downstream side of the shock. On the other hand, the predicted solution across the compression fan is more accurately predicted with the Rusanov-based blended scheme. More noticeably, the predicted solution gradients across the expansion fan are much smoother with the Rusanov-based blended scheme than the N-based blended scheme (possibly due to more dissipative nature of the Rusanov scheme). Therefore, for better stability, smaller undershoot values, and smoother solution gradients, we focus on the Rusanov-based hyperbolic blended RD schemes. Comparable results are obtained with the N-based blended schemes.

The strength of the proposed blended hyperbolic schemes is further illustrated in Fig. 11, where the exact solution is over-plotted with the predicted solution obtained on a 100×100 irregular and perturbed grid. Contour plots of the cell residual and the blending parameters, $\mathbf{\Theta}$, are also shown in this figure. Clearly, the elemental residual is well resolved throughout smooth regions. The map of the blending parameter θ_u also indicates that only small number of elements are in fact *blended* with the first-order hyperbolic scheme. This is remarkable because other works reported by the RD community presented a blending map that covers almost the majority of the domain, including the compression region, with a large θ value close to unity (e.g., see Ref. 15). Note, reducing the ϵ_θ given in Eq. (34) increases the θ_u value in the smooth region.

D. Sonic expansion

In this exercise, we examine the capability of the proposed blended schemes in accurately predicting a sonic expansion. Consider a nonlinear viscous Burgers equation, Eq. (46), with the following boundary condition

$$u(x,y) = \begin{cases} -1.0, & x \le 0, \\ +1.0, & \text{else}, \end{cases} \tag{49}$$

and $u = 0$ as the initialized solution. We first verify that the Rusanov scheme, unlike the baseline second-order RD scheme, does not require an entropy fix even on a regular grid (see Fig. 12). On the other hand, the Rusanov-based blended RD scheme, RD-B, predicts unphysical shocks on regular grid. This is because the the cell residual vanishes (resulting $\mathbf{\Theta} \to \mathbf{0}$) in the cells containing the discontinuity and thus, no signal is being sent to the corresponding nodes. Note that, the special quadrature formula proposed in Refs. 9,10 does not suffer from this shortfall observed with the trapezoidal rule used in our study. As shown in Refs. 9, 10, the cell-residual defined by the trapezoidal rule can recognize a nonlinear shock and vanish if the element has a side parallel to the shock.

However, the improved second-order RD-CC2 and the third-order RD-CC3 schemes proposed in Ref. 1, which are used in the construction of the proposed high-order blended schemes (i.e., RD-CC2-B and RD-CC3-B), are constructed based on the curvature correction terms[1] and thus, are not precisely based on the trapezoidal rule. That is, these schemes behave much better in avoiding unphysical shocks even without an entropy-fix. These are illustrated in Fig. 12.

On irregular grids, the situation is slightly better, even for the baseline RD, unless by accident, or design, the sonic expansion occurs in a region of regular grids. This is further illustrated in Fig. 13.

We can further improve the sonic expansion predictions with the help of the proposed characteristics-based nonlinear wave sensor, α, which can accurately detect the expansion region (see Sec. VI). With the detection of elements in the origin of the expansion, we employ the first-order advection-diffusion Rusanov scheme (see Sec. B) by setting $\theta_u = 1.0$ when $\alpha \le -0.9$. These results are shown in Figs. 14 and 15, respectively, for regular and irregular grids. A map of the α sensor is also shown for each of the schemes, confirming that the expansion fan is accurately predicted.

E. Accuracy verification

In this example, we consider the general advection-diffusion equation with an exact smooth exponential solution of the form:[23]

$$u(x,y) = C\cos(A\pi\eta)\exp\left(\frac{1-\sqrt{1+4A^2\pi^2\nu^2}}{2\nu}\xi\right), \tag{50}$$

where A and C are arbitrary constants, and $\xi = ax + by$ and $\eta = bx - ay$. We solve the system using the proposed blended schemes on a series of irregular and perturbed triangular grids. The order of accuracy

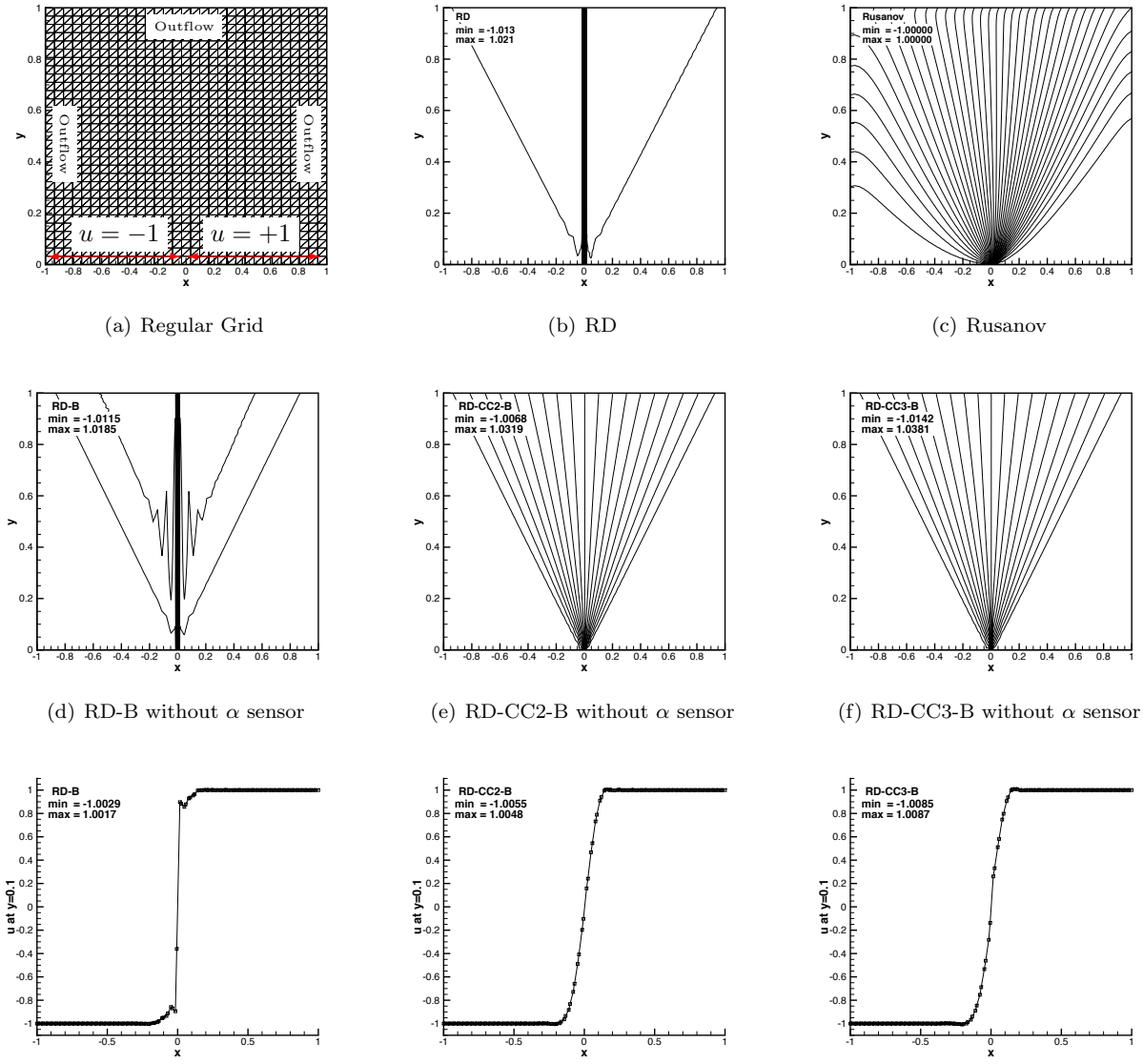

(a) Regular Grid (b) RD (c) Rusanov

(d) RD-B without α sensor (e) RD-CC2-B without α sensor (f) RD-CC3-B without α sensor

(g) RD-B without α sensor (h) RD-CC2-B without α sensor (i) RD-CC3-B without α sensor

Figure 12. Sonic expansion prediction comparison between the non-blended RD, the first-order Rusanov, and the proposed baseline and high-order blended schemes on 64×64 regular grid without activation of the α sensor ($\nu = 0.001$).

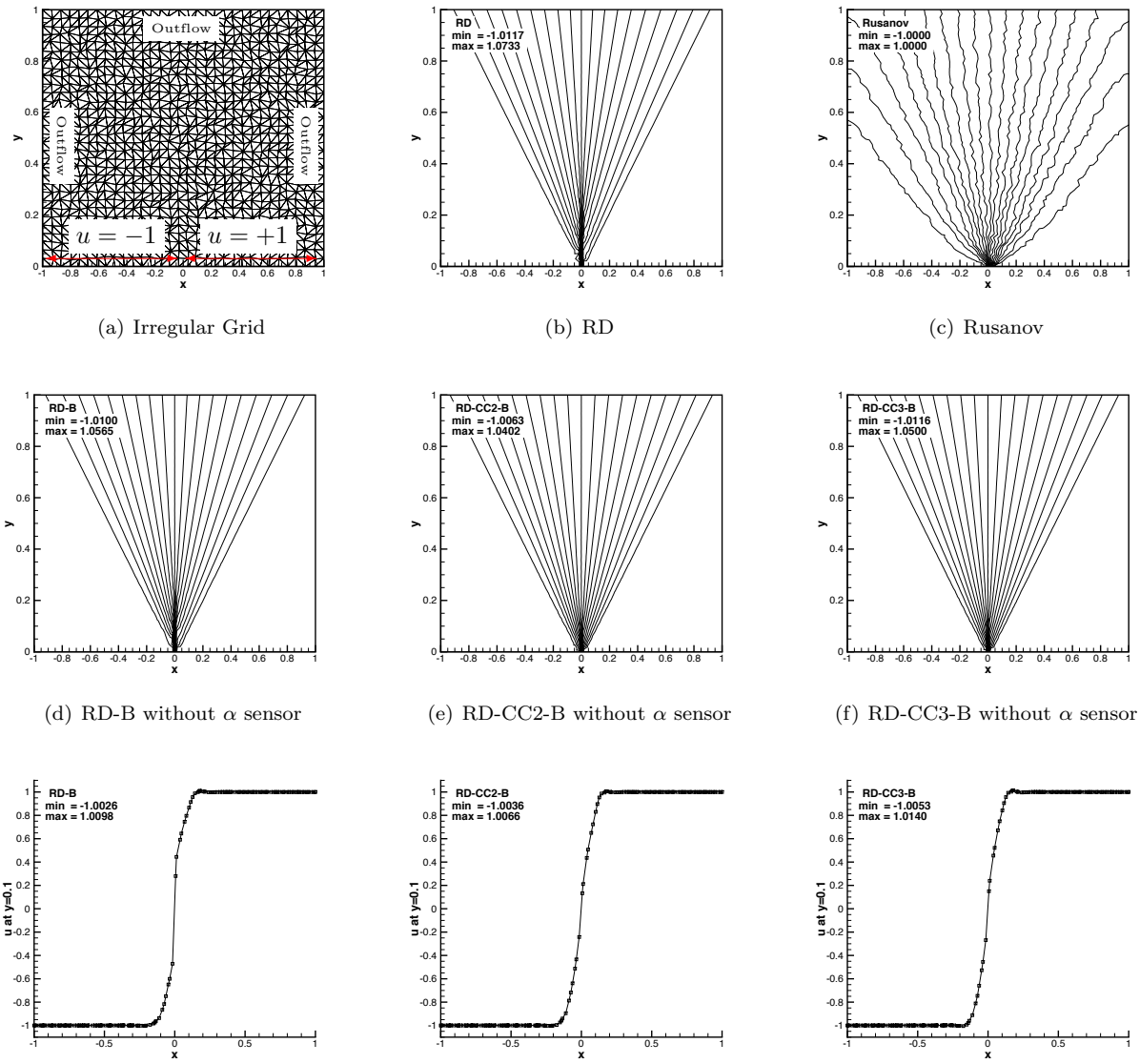

(a) Irregular Grid (b) RD (c) Rusanov

(d) RD-B without α sensor (e) RD-CC2-B without α sensor (f) RD-CC3-B without α sensor

(g) RD-B without α sensor (h) RD-CC2-B without α sensor (i) RD-CC3-B without α sensor

Figure 13. Sonic expansion prediction comparison between the non-blended RD, the first-order Rusanov, and the proposed baseline and high-order blended schemes on 64×64 irregular and perturbed grid without activation of the α sensor ($\nu = 0.001$).

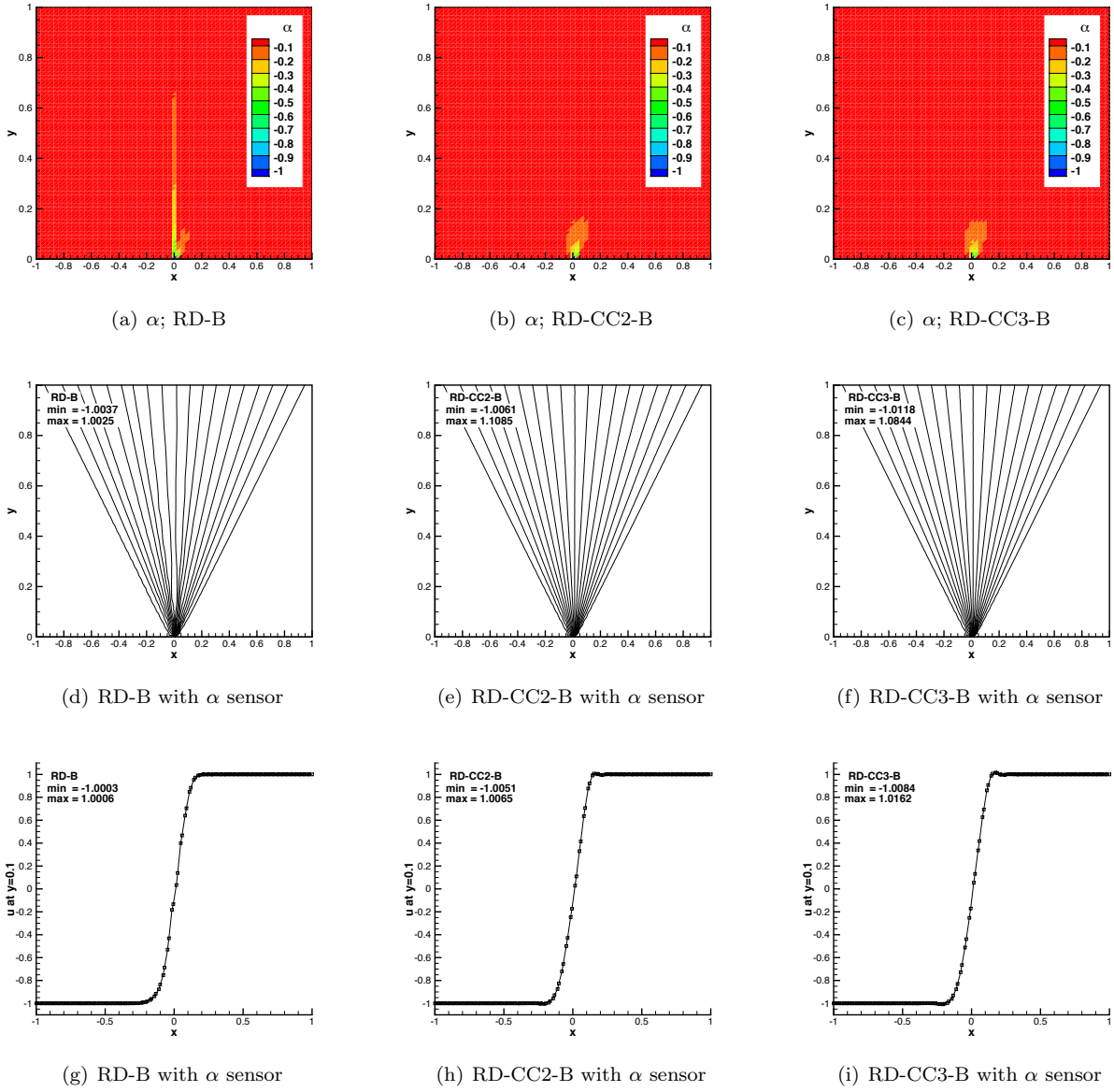

(a) α; RD-B (b) α; RD-CC2-B (c) α; RD-CC3-B

(d) RD-B with α sensor (e) RD-CC2-B with α sensor (f) RD-CC3-B with α sensor

(g) RD-B with α sensor (h) RD-CC2-B with α sensor (i) RD-CC3-B with α sensor

Figure 14. Sonic expansion prediction comparison between the baselined and the proposed blended schemes using 64×64 regular grid with activation of the α sensor as proposed in Sec. VI ($\nu = 0.001$).

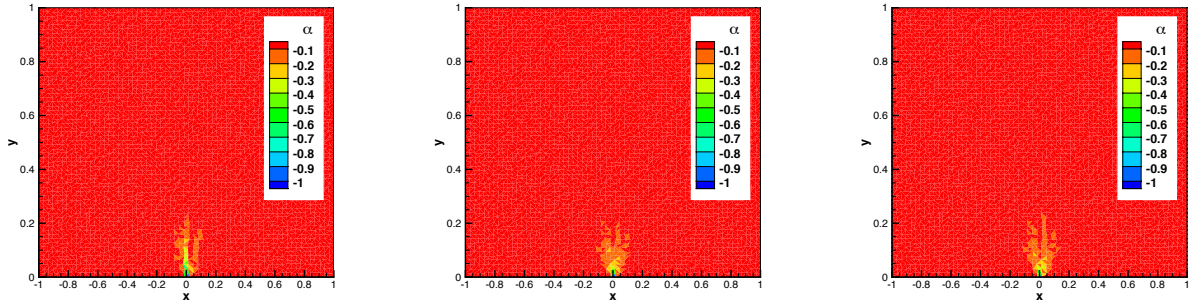

(a) α; RD-B (b) α; RD-CC2-B (c) α; RD-CC3-B

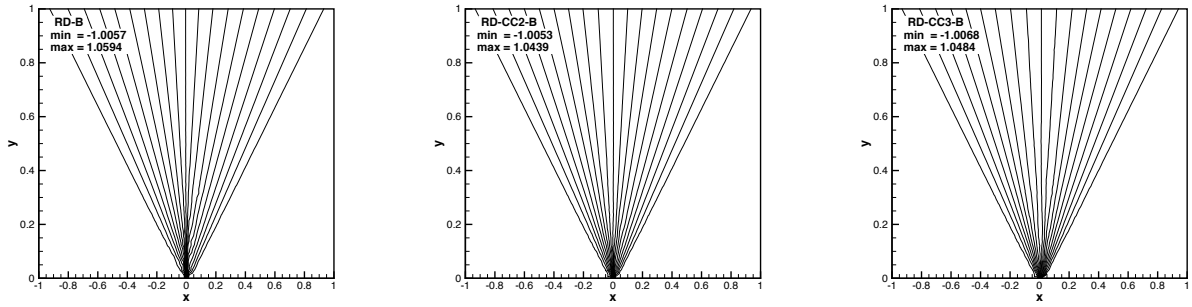

(d) RD-B with α sensor (e) RD-CC2-B with α sensor (f) RD-CC3-B with α sensor

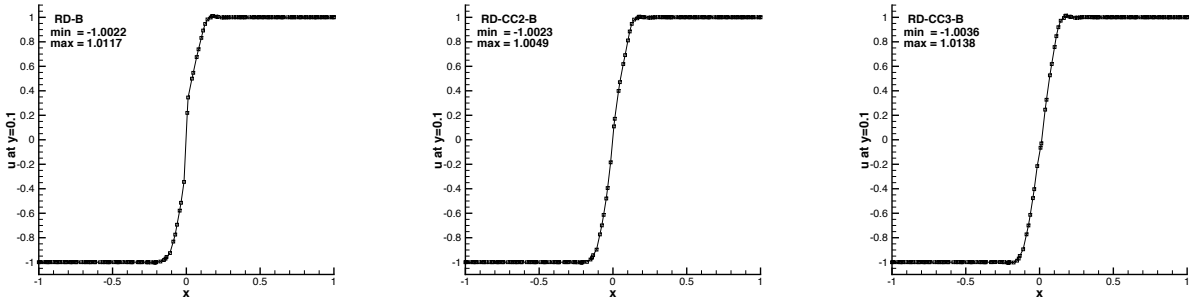

(g) RD-B with α sensor (h) RD-CC2-B with α sensor (i) RD-CC3-B with α sensor

Figure 15. Sonic expansion prediction comparison between the baselined and the proposed blended schemes using 64×64 irregular and perturbed grid with activation of the α sensor as proposed in Sec. VI ($\nu = 0.001$).

of the proposed blended schemes are shown in Fig. 16. These results confirm that the blended RD-CC2-B

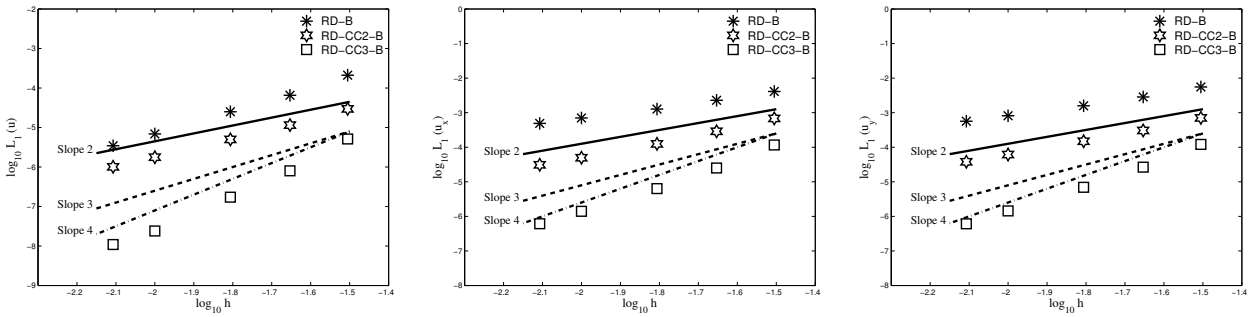

(a) u (b) u_x (c) u_y

Figure 16. Accuracy of the proposed blended schemes for the smooth exponential solution ($A = 2$, $C = -0.009$, $a = 2.0$, $b = 1.0$, $\nu = 0.01$).

scheme remains second-order for all the variables, while a uniform fourth-order solution is obtained with the blended RD-CC3-B scheme. Note that as we explained in Ref. 1, our design principle (preserving exact cubic solution) is not a necessary condition, rather is a sufficient condition to guarantee a third-order accurate solution and solution gradients. Therefore, without a mathematical proof, we can only state that the scheme is at least third-order accurate, meaning it could also be fourth-order. Note that the baseline blended RD-B scheme predicts almost second-order accurate solution gradients but the predicted gradients are extremely noisy, similar to the baselined RD scheme we showed in Ref. 1; we thus, recommend the proposed blended RD-CC2-B scheme for uniform second-order accurate solution and solution gradients.

IX. Conclusions

We have developed new second- and third-order shock-capturing blended hyperbolic residual-distribution schemes for advection-diffusion problems on irregular triangular grids. We extended the first-order advection N and Rusanov schemes to hyperbolic advection-diffusion problems. We proposed a new nonlinear blending function, and constructed high-order blended hyperbolic RD schemes. We also presented a new characteristics-based nonlinear wave sensor to accurately detect different regions of the domain (e.g., shocks, expansion, compression). We showed that the solution of the hyperbolic advection-diffusion system approaches the solution of the advection problem as the diffusion coefficient approaches zero, confirming that the hyperbolic diffusion formulation does not negatively affect the advection scheme. We showed that the developed blended schemes can accurately predict discontinuous solutions with no oscillation. In addition, we showed that these schemes also predict accurate and smooth solution gradients on irregular grids. We also demonstrated that these schemes do not suffer from entropy-violating solutions particularly when the proposed nonlinear wave sensor is used to activate the extended Rusanov scheme at the origin of the sonic expansion region. The high-order accuracy of the blended schemes was further verified on a series of irregular and perturbed grids.

Acknowledgments

The authors would like to thank the Center Chief Technology Office of NASA Langley Research Center for their support through the Center Innovation Fund (CIF) project.

References

[1]A. Mazaheri and H. Nishikawa. Improved second-order hyperbolic residual-distribution scheme and its extension to third-order on arbitrary triangular grids. *J. Comput. Phys.*, 300:455–491, 2015.

[2]R. Struijs, H. Decononck, and P.L. Roe. Fluctuation splitting schemes for the 2D euler equations. Technical Report VKI-LS 1991-01, VKI, 1991.

[3]R. Abgrall and P.L. Roe. High-order fluctuation schemes on triangular meshes. *J. Sci. Comput.*, 19:3–36, 2003.

[4]H. Deconinck, K. Sermeus, and R. Abgrall. Status of multidimensional upwind residual distribution schemes and appli-

cations in aeronautics. In *Fluids 2000 Conference and Exhibit*, AIAA Paper 2000-2328, Denver, CO, 2000.

[5]R. Abgrall. Toward the ultimate conservative scheme: following the quest. *J. Comput. Phys.*, 167:277–315, 2001.

[6]Mario Ricchiuto. *Construction and Analysis of Compact Residual Discretizations for Conservation Laws on Unstructured Meshes*. PhD thesis, Universite Libre De Bruxelles, Von Karman Institute for Fluid Dynamics, 2005.

[7]R. Abgrall. Essentially non-oscillatory residual distribution schemes for hyperbolic problems. *J. Comput. Phys.*, 214:773–808, 2006.

[8]J. Dobes and H. Deconinck. Second order blended multidimensional upwind residual distribution scheme for steady and unsteady computations. *J. Comp. App. Math.*, 215:378–389, 2008.

[9]H. Nishikawa, M. Rad, and P. L. Roe. Grids and solutions from residual minimisation. In N. Satofuka, editor, *Computational Fluid Dynamics 2000*, pages 119–124. Springer-Verlag, 2000.

[10]H. Nishikawa. Adaptive-quadrature fluctualing-spliting schemes for the Euler equations. *Int. J. Numer. Meth. Fluids*, 57(1):1–12, 2008.

[11]A. Bonfiglioli, M. Grottadaurea, R. Paciorri, and F. Sabetta. An unstructured, three-dimensional, shock-fitting solver for hypersonic flows. *Computer and Fluids*, 14:21–39, 2013.

[12]R. Pepe, A. Bonfiglioli, R. Paciorri, A. Lani, J.G. Mena, and C.F. Olliver-Gooch. Towards a modular approach for unstructurted shock-fitting. In *6th European Conference on Computational Fluid Dynamics VI*, Barcelona, Spain, 2014.

[13]R. Pepe, A. Bonfiglioli, A. D'Angola, G. Colonna, and R. Paciorri. An unstructure shock-fitting solver for hypersonic plasma flows in chemical non-equilibrium. *Comp. Phys. Comm.*, doi:10.1016/j.cpc.2015.06.005, 2015.

[14]K. Sermeus and H. Deconinck. An entropy fix for multi-dimensional upwind residual distribution schemes. *Computer and Fluids*, 34:617–640, 2005.

[15]Kurt Sermeus. *Multi-dimensional upwind discretization and application to compressible flows*. PhD thesis, Universite Libre De Bruxelles, Von Karman Institute for Fluid Dynamics, 2013.

[16]A. Mazaheri and H. Nishikawa. Very efficient high-order hyperbolic schemes for time-dependent advection-diffusion problems: Third-, fourth-, and sixth-order. *Computers and Fluids*, 102:131–147, 2014.

[17]P.L. Roe and D. Sidilkover. Optimum positive linear schemes for advection in two and three dimensions. *SIAM J. Num. Anal.*, 29:1542–1568, 1992.

[18]D. Sidilkover and P.L. Roe. Unifaction of some advection schemes in two dimensions. Technical Report ICASE 95-10, NASA, 1995.

[19]A. Mazaheri and H. Nishikawa. High-order hyperbolic residual-distribution schemes on arbitrary triangular grids. In *Proc. of , 22nd AIAA Computational Fluid Dynamics Conference*, AIAA Paper 2015–2445, Dallas, Texas, 2015.

[20]H. Nishikawa. A first-order system approach for diffusion equation. II: Unification of advection and diffusion. *J. Comput. Phys.*, 229:3989–4016, 2010.

[21]R. Abgrall and M. Mezine. Construction of second-order accurate monotone and stable residual distribution schemes for steady flow problems. *J. Comput. Phys.*, 195:474–507, 2004.

[22]H. Nishikawa. A first-order system approach for diffusion equation. I: Second order residual distribution schemes. *J. Comput. Phys.*, 227:315–352, 2007.

[23]H. Nishikawa and P.L. Roe. On high-order fluctuation-splitting schemes for Navier-Stokes equations. In C. Groth and D.W. Zingg, editors, *Computational Fluid Dynamics 2004*, pages 799–804. Springer-Verlag, 2004.

[24]H. Harten and J.M. Hyman. Self-adjusting grid methods for one-dimensional hyperbolic conservation laws. *J. Comput. Phys.*, 50:235–269, 1983.

[25]W.A. Wood and W.L. Kleb. 2D/Axisymmetric formulation of multi-dimentional upwind scheme. In *15th AIAA Computational Fluid Dynamics Conference*, AIAA Paper 2001-2630, Anaheim, CA, 2001.